Suppressing the Folding of Flowing Viscous Jets Using an Electric Field

Tiantian Kong (孔湉湉),[1,2] Zhou Liu (刘洲),[1,3] Liqiu Wang (王立秋),[1,2,*] and Ho Cheung Shum (岑浩璋)[1,3,†]

[1]*The University of Hong Kong, Haking Wong Building, Department of Mechanical Engineering, Hong Kong*
[2]*HKU-Zhejiang Institute of Research and Innovation (HKU-ZIRI), Hangzhou, Zhejiang 311100, China*
[3]*HKU-Shenzhen Institute of Research and Innovation (HKU-SIRI), Shenzhen, Guangdong 518000, China*

(Received 2 June 2014; revised manuscript received 17 February 2015; published 26 March 2015)

In this work, we study the folding and unfolding of flowing viscous jets by imposing an electric field. We demonstrate that a folded viscous jet can be induced to unfold through jet widening in a sufficiently strong electric field. The folded jets unfold above a critical slenderness, which increases as the jet capillary number increases. Our systematic elucidation of the mechanisms behind the controlled folding has important implications on processes such as nozzle designs for industrial applications that rely on the manipulation of high-speed viscous jets, including liquid dispensing, printing, and food processing.

DOI: 10.1103/PhysRevApplied.3.034010

I. INTRODUCTION

The deformation of fluid streams occurs on the macroscale as well as on the micro- and nanoscale, and has attracted scientists for centuries [1]. Formation of geographic structures, such as the two-layer mantle, may be attributed to the folding of viscous fluids [2,3]; buckling and folding of viscous solutions are also observed in food processing [4] and polymer processing [5–8]. Liquid jets with large-enough viscosity can behave like elastic rods [9–12]. For example, viscous jets of honey and shampoo fold like elastic ropes when they are dripped onto a surface. The compressive stress along the axial direction [3,11–21], resulting from jet deceleration (for instance, when the jet hits a plate [3,9,11,12,17,18,22,23]or enters a diverging channel [24–26]), is the driving force of folding. The folding of a viscous jet can be characterized by the folding frequency and amplitude, which are influenced by the diameter, velocity, and kinematic viscosity of the jet [3,11,12,18,20,23–25]. The ability to control and manipulate the morphology of viscous jets is crucial for applications such as electrospinning [6,27,28].

When a viscous filament is compressed, it bends or becomes thicker to satisfy mass conservation [10]. Analogous to Euler elastic buckling [10], only a sufficiently slender viscous filament can bend [10]. This analogous folding of a liquid filament only happens at sufficiently large capillary number $\mathrm{Ca} = \mu v/\gamma$, where μ, v, γ are viscosity, velocity, and surface tension of the viscous filament, respectively. At small Ca, the significant capillarity effect favors the formation of a straight jet, which has a smaller interfacial area than a folded jet. Therefore, capillary number Ca and filament slenderness $\varepsilon \equiv D/L$, where D and L are the average diameter and length of the filament, respectively, are the two independent criteria to predict bending of a viscous filament [10]. With a sufficiently large Ca and small ε, a quiescent viscous filament can bend. These criteria imply that, to unfold a folded, flowing viscous jet, one can either decrease Ca by reducing velocity [25] or increase ε. However, due to their high resistance against deformation, the diameter of a viscous jet changes only slightly even when the volumetric flow rate is varied to a large extent [29]. Thus, it is difficult to change the slenderness ε of a viscous jet hydrodynamically. It remains difficult to straighten folded viscous jets flowing at high velocity, presenting a challenge for applications that rely on the dispensing of viscous liquids.

In the present work, we study the folding and unfolding of a flowing viscous jet under an electric field. We demonstrate that a sufficiently strong electric field can induce the folded viscous jet to unfold. The imposed electric field causes an axial and a normal electric stress on the jet surface. We elucidate that the unfolding of the jet is mainly due to the normal electric stress, leading to jet widening. Moreover, the folded jet unfolds above a critical slenderness, which increases as the jet capillary number increases. By enabling precise control over the degree of viscous folding, our study has important implications for industrial applications that rely on the manipulation of high-speed viscous jets, such as liquid dispensing, printing, and food processing.

II. METHODS

A. Fabrication of microchannels

We form our microchannel by inserting a tapered, round glass capillary (World Precision Instruments) into a square glass capillary (AIT Glass). The round capillary, with inner and outer diameters of 0.58 mm and 1 mm, respectively, is

*Corresponding author.
lqwang@hku.hk
†Corresponding author.
ashum@hku.hk

tapered by a micropipette puller (Sutter P-97) and then polished with sandpaper to a diameter of 100–200 μm. The square capillary has an inner diameter of 1.05 mm. Both capillaries are fixed on a microscopic glass slide using 5-min epoxy (Devcon, VersaChem). The liquid phases are injected into the microchannels through metal syringe needles and polyethylene microtubing (Scientific Commodities).

B. Composition and properties of liquid phases

The immiscible liquids used in our experiments are aqueous-oil systems and aqueous two-phase systems. For the aqueous-oil systems, we use a mixture of glycerin, a 1-wt % potassium chloride (KCl) water solution, and 2-wt % Tween 20, as the aqueous viscous phase; dodecane with 3-wt % Span 80 is used as the less-viscous outer oil phase. The viscosity of the inner phase is 0.579 Pa s. The molar concentration of KCl in its water solution is varied to modify the electrical conductivity of the aqueous viscous phases. The combination of surfactants Tween 20 and Span 80 can lower the interfacial tension between oil and water beyond solutions of pure Tween 20 or Span 80 alone [30].

For the aqueous two-phase systems, we use a mixture of 10-wt % dextran ($M_w = 500\,000$) and 10-wt % dextran sodium sulfate ($M_w = 500\,000$) as the viscous inner phase, and 13-wt % polyethylene glycol ($M_w = 6000$) as the less-viscous outer phase.

The electrical conductivities of all liquid phases are measured using a conductivity meter (Eutech, CONT 610). The conductivities of the inner phase in the aqueous-oil system are 0.1 μS/cm, 1.29 μS/cm, 3.73 μS/cm, and 31.8 μS/cm, depending on the molar concentration of KCl; while the conductivity of the outer oil phase is smaller than 10^{-6} μS/cm. In the aqueous two-phase system, the electrical conductivities of inner and outer phases are 8300 μS/cm and 50.9 μS/cm, respectively.

All the interfacial tensions are measured using a spinning drop tensiometer (KRÜSS, SITE100). The interfacial tensions of the aqueous-oil and aqueous two-phase systems are measured to be 1.3 mN/m and 0.072 mN/m, respectively. Based on the measurements by a microfluidic viscometer (RheoSense μVISC), the viscosities of viscous inner phases in aqueous-oil and aqueous two-phase systems are 0.579 Pa s and 0.6 Pa s, respectively.

C. Formation of viscous jets

We form the viscous jet in another less-viscous immiscible liquid using a co-flow microchannel (Fig. 1). The viscous inner liquid L_1 with flow rates Q_1 flows through the tapered round capillary and then into the square one. The less-viscous outer liquid L_2 with flow rate Q_2 flows through the gap between the round and square capillaries, in the same direction. The motion of the viscous jet is recorded under an inverted microscope (Motic AE2000) using a high-speed camera (Phantom v9.1).

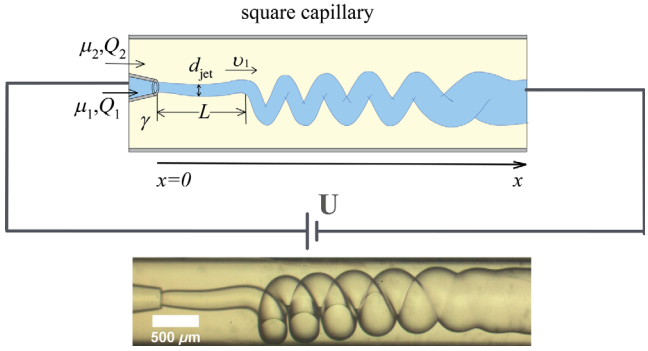

FIG. 1. Schematic of the experimental setup: a viscous jet is formed in an immiscible liquid using a microfluidic co-flow device [32]. The inset optical microscopic image shows a folding jet after exiting the nozzle with a diameter of 150 μm. The folding jet does not touch or wet the microchannel walls in our experiments.

The electric field is introduced through metal needles at the inlet of the viscous inner phase and the outlet of the microfluidic device using a high-voltage power supply of potential drop U (Fig. 1). Since the conductivity of the inner phase k_1 is at least 2 orders of magnitude larger than the outer phase k_2 in all the liquid-liquid systems, the potential drop U mainly falls on the viscous jet.

To characterize the geometry of the folding jet, we define the jet slenderness as $\varepsilon = D/L$, where D and L are the average diameter and length of the jet between the nozzle ($x = 0$) and the position the jet starts to fold ($x = l$) (Fig. 1) (see the Supplemental Material [31]).

The significantly larger viscosity of the inner phase μ_1, compared to that of the outer phase μ_2, ensures a negligible viscous effect from the outer phase. The low interfacial tensions, on the order of 1 mN/m for aqueous-oil systems and 10^{-2} mN/m for systems formed by two immiscible aqueous phases, ensure that the viscous effect dominates over capillarity. Gravitational and inertial forces are negligible here since the Bond number and Reynolds number (dimensionless ratios of gravitational over surface tension effects and inertial over viscous forces, respectively) are both on the order of 10^{-2}. Moreover, the Ohnesorge number (defined by $\mathrm{Oh} = \mu/\sqrt{\rho\gamma l}$, where ρ, l are the density and characteristic length of the liquid) measures the relative importance of viscous over inertial and surface tension effects. In our system, Oh is on the order of 10; thus, the viscous effect dominates over inertial and surface tension effects.

III. RESULTS

A. Jet behaviors in the absence of electric stress

Under the configuration of our microdevice, the viscous jet exits the nozzle, and enters a wide channel with a higher velocity than that of the surrounding fluid, resulting in jet deceleration. The deceleration gives rise to an axial

compressive stress due to the difference in the axial velocity, which induces folding [24–26,33].

The axial stress T consists of the effects of surface tension, viscous stress, and an imposing electric stress. The viscous stress results from the uneven axial velocity distribution in the jet [Eq. (1)] [21,34],

$$T = \frac{\gamma}{d_{\text{jet}}} + 3\mu_1 \frac{dv_1}{dx} + S_e, \tag{1}$$

where γ represents the interfacial tension of the liquid-liquid interface; x denotes the axial direction; $d_{\text{jet}}, \mu_1, v_1$ are the local diameter, viscosity, and velocity of the viscous jet, respectively; and S_e denotes the imposing axial electric stress [34]. The viscous jet is under compression when $T < 0$ and under tension when $T > 0$.

We relate this compressive stress T to capillary number Ca. Assuming the viscous inner fluid at the center is lubricated by the less-viscous outer fluid, we can rewrite the velocity of the jet along the axial direction as $v_1 = 4Q_1/\pi d_{\text{jet}}^2$; thus Eq. (1) becomes

$$6\text{Ca}\frac{d(d_{\text{jet}})}{dx} + S_e\frac{d_{\text{jet}}}{\gamma} - 1 > 0, \tag{2}$$

and this equation gives the first necessary criterion for folding, where $[d(d_{\text{jet}})/dx]$ is the dilation gradient.

Assuming that the jet is axisymmetric, from the nozzle ($x = 0$) to where the jet starts to fold ($x = l$), the dilation gradient of the jet can be expressed as

$$\frac{d(d_{\text{jet}})}{dx} = 2\varepsilon - 2\frac{d_{\text{nozzle}}}{L}. \tag{3}$$

For folding to be observed, the characteristic buckling time $\tau_0 \sim D^2/Lv$ [10], where v is the average velocity of the jet and can be estimated from $v \sim (4Q/\pi D^2)$, must be smaller than the characteristic time scale of fluid flow based on viscous stress $\tau_h \sim \mu L/\gamma$, as viscous stress dominates over inertial and surface force ($\text{Oh} = \sqrt{\text{We}}/\text{Re} \sim 10$) [1]. This requirement necessitates $\varepsilon_c \sim \text{Ca}^{1/2}$, representing the slenderness criterion for folding (see the Supplemental Material [31]).

In the absence of electric stress ($S_e = 0$), we summarize the compression and slenderness criteria in a static phase diagram (Ca, ε) [Figs. 2(a) and 2(b)]. When Eq. (2) [see the yellow dotted line in Fig. 2(b)] is not fulfilled, the jet is stretched, as shown on the left side. The unfolding region represents jets that are under compression but not sufficiently slender, as denoted by the open squares [Fig. 2(b)]. With both criteria fulfilled, folding is observed [see solid squares in Fig. 2(b)]. Moreover, with a certain capillary number, the folded jet will unfold when the slenderness is above a critical value. With a larger capillary number, the critical slenderness of the jet that leads to unfolding is larger.

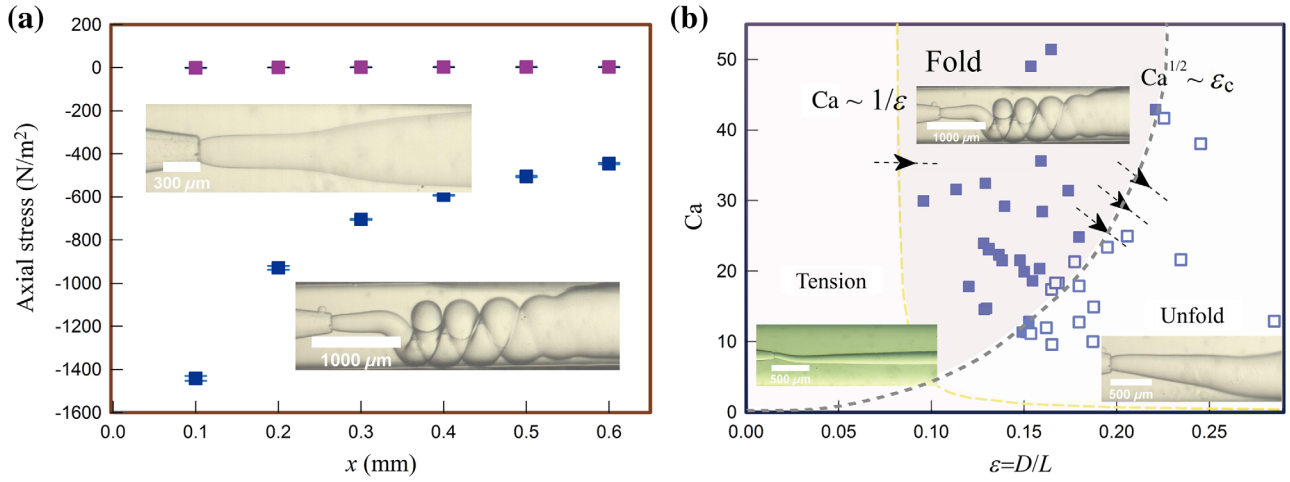

FIG. 2. (a) Plot of axial stress T at different locations of the jet calculated by Eq. (1): the jet folds when $T < 0$ and the jet does not fold when $T > 0$. The straight jet is made up of a mixture of glycerin, 20-wt % water, and 2-wt % Tween 20, with a viscosity of 0.015 Pa s. For the folding jet, the weight ratio of water decreases from 20-wt % to 2-wt % and thus the viscosity increases to 0.579 Pa s. For both jets, the outer oil phase is dodecane with 3-wt % Span 80. (b) Phase diagram for the viscous folding jet. The left side is the region where the jet is in tension; the middle is the folding region, where both compression and slenderness criteria are fulfilled; the right side is the region where compressed jets do not fold. The yellow dotted lines represents the compression criterion $6\text{Ca}[2\varepsilon - (2d_{\text{nozzle}}/L)] > 1$ by Eq. (2) and Eq. (3), where $d_{\text{nozzle}}/L = 8 \times 10^{-2} \pm 8 \times 10^{-3}$ is estimated experimentally. The gray dotted line represents the slenderness criterion $\varepsilon \sim \text{Ca}^{1/2}$. Each point corresponds to an experiment done using aqueous-oil systems with different viscosities and conductivities; folding is denoted by the solid squares while the absence of folding is denoted by empty squares. The orifice size of the jet in "Tension" is 100 μm while that of jets in "Fold" and "Unfold" is 160 μm. Arrows denote the transition between the different regions of "Tension", "Fold," and "Unfold." This static diagram is obtained without the electric stress ($S_e = 0$).

B. Transition from jet folding to unfolding with electric stress

The axial electric stress S_e can be either compressive or tensile depending on its direction relative to that of the flow. If the axial electric stress is compressive, an enhanced folding is expected. In contrast, a sufficiently large tensile stress can potentially straighten and thus unfold the folded jet.

When an electric field parallel to the flow direction is applied, an axial compressive electric stress on the jet surface arises. As a potential drop U falls onto the viscous jet, the electric stress exerted on the dilated jet interface occurs with a slope α to the axial direction x. Since the direction of the electric field is almost parallel to the channel axis, the electric field intensity imposed on the viscous jet can be approximated by its tangential component E_t [Fig. 3(a)]. This E_t accelerates positive charges and decelerates negative charges, leading to the accumulation of negative charges at the diverging interface. Thus, the charged jet interface is subjected to a tangential electric field E_t, which gives rise to

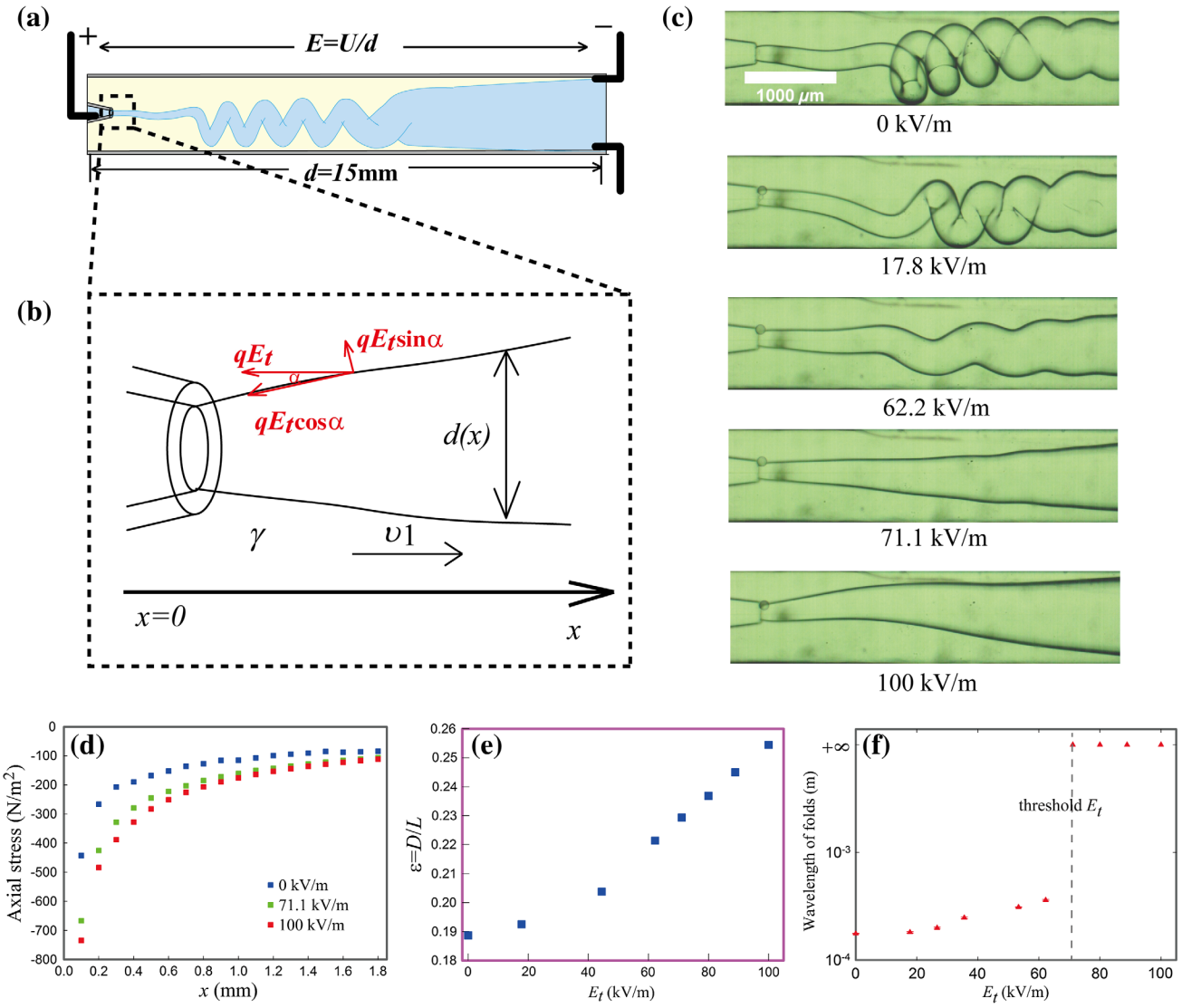

FIG. 3. (a) Schematic showing the electric field applied on the viscous jet. (b) Schematic of the electric stress exerted on the jet interface near the nozzle. (c) A series of optical microscope images shows that the viscous jet folds less vigorously and becomes wider as electric field intensity increases; at a threshold value (71.1 kV/m), the jet becomes straight, as shown in the fourth image. The diameter of the straight jet also expands with the increase of electric field intensity. The orifice in this series of images is 160 μm. The increase of the electric field has two effects on the viscous jet: (d) the axial compressive stress increases and (e) ε becomes larger with the increase of applied voltage due to the widening of the jet. (f) A plot of the electric field intensity as a function of the folding wavelength. Above the threshold field intensity, the wavelength becomes infinite, which indicates the unfolding of jet. The viscous jet in this figure is a mixture of glycerin, 2-wt % water, and 2-wt % Tween 20, with a viscosity of 0.579 Pa s, while the outer oil phase is dodecane with 3-wt % Span 80. The flow rates of inner and outer phase are 8 ml/h and 10 ml/h, respectively. Their interfacial tension is 1.3 mN/m.

electric interfacial stress [35]. This electric interfacial stress (which can be calculated using the surface charge density q and field intensity E_t, $\tau = qE_t$) is opposing the flow. It has two components; one is parallel to the interface $qE_t \cos\alpha$, which increases the compressive stress; the other is normal to the interface $qE_t \sin\alpha$, which tends to pull the interface outward [Fig. 3(b)]. This compressive electric stress is different from the tensile electric stress in typical electrospinning, which leads to dramatic jet thinning and increase of q, subsequently resulting in jet whipping [36–38].

This axial compressive electric stress increases with an increasing U [Figs. 3(c) and 3(d)], which should enhance the folding. Surprisingly, we observe less folding as U increases [Fig. 3(c)] [31]. This result is counterintuitive, as only tensile stress is in the right direction to reduce the degree of folding. Moreover, as the potential drop U increases above a threshold value U_c, folding disappears. The folded jet unfolds and becomes completely straight. Meanwhile, we observe evident jet widening with increasing U. Even after the jet is unfolded, the straightened jet continues to widen as U increases from U_c (see the Supplemental Material [31]).

We attribute this unexpected unfolding phenomenon to the jet widening, due to the normal component of the electric stress. This normal electric stress pulls the interface outward and thus widens the jet. The increase in the jet diameter leads to a corresponding increase in ε [Fig. 3(e)], and eventually results in the transition from the folding to the unfolding region [Fig. 2(b)].

Therefore, the application of an electric field has two competing effects: it enhances the axial compressive stress, which should enhance the folding; it also widens the jet, leading to the transition to unfolding. At small U, although the jet is wider, the compressive stress also becomes larger and the jet is still folded [Figs. 3(c)–3(e)]. However, at a threshold U_c, the jet becomes so wide that the increased compressive stress fails to fold it; the jet becomes straight and the wavelength of folds approaches infinity [Figs. 3(c) and 3(f)]. An increase in U of the straightened jet leads to a further increase in jet diameter [Fig. 3(e)]. When U is gradually reduced to 0 V, the jet becomes thinner and starts to fold again (for details, see the Supplemental Material [31]).

C. Jet expansion in the normal direction

The jet-widening effect prevails over the enhanced compression effect due to the electric stress, resulting in jet unfolding. Thus, electrically dilating the jet is effective for suppressing the folding instability of the flowing viscous jet. This dilation is controlled by the balance of the electric stress exerted on the interface and the interfacial tension. This balance can be described using the electric capillary number $\mathrm{Ca}_{\mathrm{electric}} = qEd_{\mathrm{jet}}/\gamma$, where q, E, d_{jet} are the charge density, local field intensity, and jet diameter, respectively [39]; γ represents the interfacial tension of the jet. The electric capillary number indicates the deformability of the jet by electric stress. Under a low $\mathrm{Ca}_{\mathrm{electric}}$, a jet shows no response to electric field while at a high $\mathrm{Ca}_{\mathrm{electric}}$, a jet deforms under the same electric field [29]. Furthermore, we hypothesize that a higher electric capillary number may lead to a larger expansion of the jet diameter $\delta = (d_{\mathrm{jet}}{}^{*} - d_{\mathrm{jet}})/d_{\mathrm{jet}}$, where $d_{\mathrm{jet}}{}^{*}$ is the jet diameter after deformation due to the electric stress [31]. For instance, we observe that a jet becomes wider as the applied field intensity increases [Fig. 3(e)]. Moreover, the deformation of the jet is significantly influenced by its interfacial tensions, which are inversely proportional to $\mathrm{Ca}_{\mathrm{electric}}$. For systems with an ultralow interfacial tension, such as an aqueous two-phase system with $\gamma = 0.072$ mN/m, an electric field intensity of 0.7 kV/m leads to a 40% expansion in diameter, while for an aqueous-oil system with $\gamma = 1.3$ mN/m, the electric field intensity needs to be over 80 kV/m to achieve the same expansion (see the Supplemental Material [31]). Electrical conductivity has no significant influence on the jet expansion, nor on the threshold voltage from folding to unfolding, as exhibited by the lack of observable changes in the result as the electrical conductivity of the viscous jet is changed from 10^{-1} μS/cm to 10^{2} μS/cm, while keeping all other conditions constant [31].

To quantify the influence of normal electric stress over interfacial tension on the expansion of jet diameter, the charge density at the jet interface q is needed to determine the electric stress. To determine q at jet interface, we introduce an electric field by inserting two electrodes near the nozzle in the microfluidic device [Figs. 4(a) and 4(b)]; the folded jet is positively charged and these two electrodes are negatively charged without directly contacting the jet. The electrical conductivity of the inner jet is at least 2 orders of magnitude larger than that of the outer phase. Thus, we can treat the interface of the inner jet as equipotential. Therefore, the jet interface is positively charged with the interior electric field intensity equal to zero [Fig. 4(b)]. By Gauss's law, the interface charge density q can be calculated using the dielectric constant of the fluid and the normal component E_n, responsible for attracting charges to an interface, $q = \varepsilon_0\varepsilon_1 E_n$ [27]. The normal and tangential electric stresses on the jet interface are $\varepsilon_0\varepsilon_1 {E_n}^2$ and $\varepsilon_0\varepsilon_1 E_n E_t$, respectively [40]. Therefore, the ratio of electric stress $\varepsilon_0\varepsilon_1 {E_n}^2$ over interface tension γ/d_{jet} can be described by electric capillary number, $\mathrm{Ca}_{\mathrm{electric}} = \varepsilon_0\varepsilon_1 {E_n}^2 d_{\mathrm{jet}}/\gamma$, where ε_0 and ε_1 are the dielectric constants of the vacuum and the viscous jet, respectively [39]. We find experimentally that the expansion of jet diameter is quite subtle when the electric stress is small compared to interfacial tension, such as when $\mathrm{Ca}_{\mathrm{electric}} < 0.5$, and grows almost linearly with the increasing ratio of electric stress over interfacial tension ($\mathrm{Ca}_{\mathrm{electric}} > 0.5$). By tuning the jet diameter and electric field intensity to vary $\mathrm{Ca}_{\mathrm{electric}}$, all experimental data collapse onto a straight line with a constant slope [Fig. 4(c)]. This result confirms our hypothesis that large electric stress over

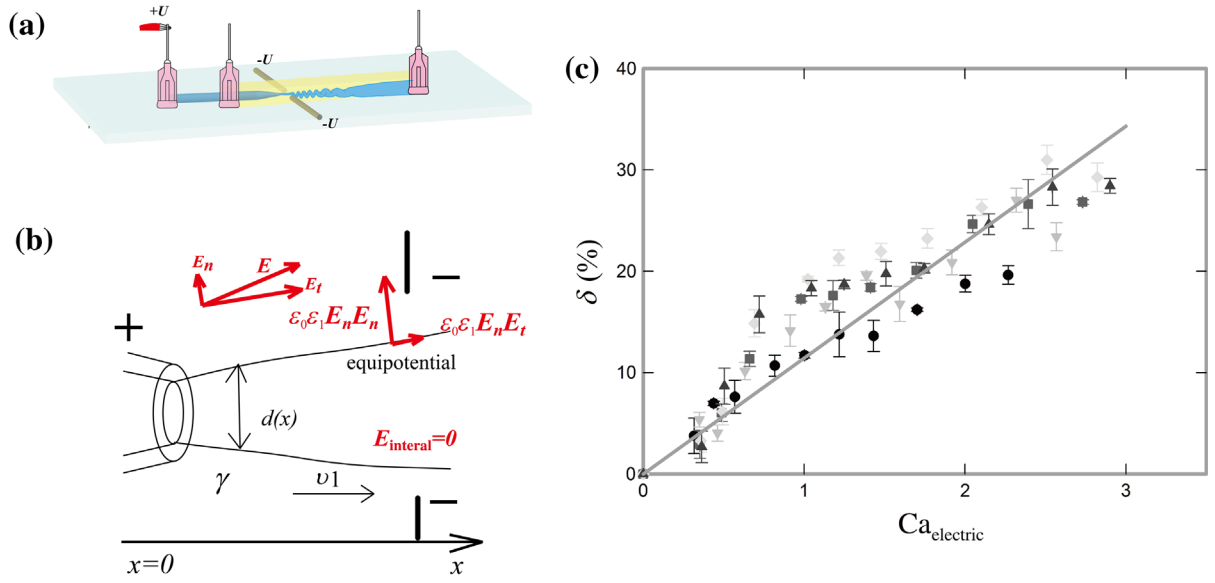

FIG. 4. (a) Schematic showing that the electric field is introduced by connecting the inlet for a viscous jet and the two metal needles inserted near the nozzle to the two ends of a power supply. (b) Schematic showing the electric stress exerted on the jet interface. (c) A plot of measured jet-diameter expansion δ as a function of calculated $Ca_{electric}$. By tuning parameters that affect $Ca_{electric}$, such as local jet diameter and field intensity, different experimental data represented by solid symbols collapse onto a solid line, which is a power-law fit with an exponent $n = 1$, and a slope approximately 11.443. The different symbols correspond to different jet diameters: $d_{jet} =$ 132.36 μm (○), $d_{jet} = 140.3$ μm (▽), $d_{jet} = 148.28$ μm (□), and $d_{jet} = 154.37$ μm (△), and $Ca_{electric}$ is varied by changing the field intensity for jets of the same diameter. The data are obtained using aqueous two-phase systems. The inner phase is a mixture of 10-wt % dextran ($M_w = 500\,000$) and 10-wt % dextran sodium sulfate ($M_w = 500\,000$), while 13-wt % polyethylene glycol ($M_w = 6000$) is the less-viscous outer phase. The flow rates of the inner and outer phase are 6 ml/h and 2 ml/h, respectively. Their interfacial tension is 0.072 mN/m.

interface tension $Ca_{electric}$ leads to a large expansion ratio of the jet diameter δ. Moreover, in the absence of other significant forces, $Ca_{electric}$ scales with δ.

To analyze the relationship between δ and $Ca_{electric}$ theoretically, we perform a force balance at the radial direction of the jet. The radial velocity of the jet is zero in the absence of any electric field, indicating that each point of the jet interface at the radial direction is in static equilibrium. The normal component E_n induces an electrostatic pressure $\Delta P_E \sim \varepsilon_0\varepsilon_1 {E_n}^2$ on the jet interface due to the interfacial charges. The jet interface is pulled outward; the jet diameter d_{jet} increases by $d(d_{jet})$, and reaches static equilibrium again [Fig. 3(c)]. The expansion of jet diameter due to the electrostatic pressure is expressed as $\delta = d(d_{jet})/d_{jet}$. At any point of the jet interface under a certain electric stress, the static equilibrium indicates a zero net force in the radial direction. The reduced capillary pressure $\Delta P_C \sim d(-\gamma/d_{jet}) = (\gamma/{d_{jet}}^2)d(d_{jet})$ due to the increase in jet diameter $d(d_{jet})$ is compensated for by the induced electrostatic pressure ΔP_E, which can be expressed as

$$\varepsilon_0\varepsilon_1 {E_n}^2 \sim (\gamma/{d_{jet}}^2)d(d_{jet}). \quad (4)$$

Therefore, the jet expansion ratio should scale with the electric capillary number, $\delta \sim Ca_{electric}$, in excellent agreement with the experimental data [Fig. 4(c)]. From this scaling relationship, the electrical conductivity has negligible influence on the jet expansion, and thus does not affect the threshold voltage from folding to unfolding (see the Supplemental Material [31]). This conclusion is in agreement with our experimental observations. The shear stress from the outer phase, on the scale of 10^{-13} N/m^2, is significantly smaller than the electric stress or the capillary pressure, and can thus be neglected. The ability to predict expansion ratios of jets from their electric capillary numbers facilitates implementation of the proposed approach for manipulating viscous jets in applications involving high-speed liquid dispensing.

IV. CONCLUSION

In conclusion, the folding of flowing viscous jets can be suppressed by increasing the jet diameter. Despite the presence of an axial compressive stress, the resultant jet can unfold and turn into a straight one. This unfolding phenomenon can be achieved by applying an electric stress on the jet surface. The normal electric stress pulls the charged interfaces of the jet outward and thus widens the jet. We show that viscous jet dynamics can be efficiently controlled by our approach, which is difficult to achieve hydrodynamically. The folding to unfolding demonstrated

in both aqueous-aqueous and aqueous-oil systems implies that this phenomenon is general across systems with different electrical conductivities, viscosities, and interfacial tensions, and the results can be extended to common two-phase systems, such as liquid-gas systems. These insights can inspire new designs of setups for nozzles in dispensing and printing of viscous liquids.

ACKNOWLEDGMENTS

Tiantian Kong and Zhou Liu contributed equally to this work. We would like to thank Thomas Cubaud and Alban Sauret for stimulating discussions. This research was supported by the Early Career Scheme (Grant No. HKU 707712P), the General Research Fund (Grants No. HKU 719813E, No. 717613E, No. 718111E, No. 17304514, and No. 17207914) sponsored by the Research Grants Council of Hong Kong, the Basic Research Program-General Program (Grants No. JC201105190878A) from the Science and Technology Innovation Commission of Shenzhen Municipality, the General Program (Grants No. 21476189/B060201), and the Young Scholar's Program (Grant No. NSFC51206138/E0605) from the National Natural Science Foundation of China as well as the Seed Funding Program for Basic Research (Grant No. 201211159090, No. 201311159187, and No. 201411159074) and Small Project Funding (Grant No. 201109176165) from the University of Hong Kong. This research is also supported in part by the Zhejiang Provincial, Hangzhou Municipal, and Lin'an County Governments.

[1] J. Eggers and E. Villermaux, Physics of liquid jets, Rep. Prog. Phys. **71**, 036601 (2008).
[2] R. W. Griffiths and J. S. Turner, Folding of viscous plumes impinging on a density or viscosity interface, Geophys. J. Int. **95**, 397 (1988).
[3] N. M. Ribe, M. Habibi, and D. Bonn, Liquid rope coiling, Annu. Rev. Fluid Mech. **44**, 249 (2012).
[4] M. Tome and S. McKee, Numerical simulation of viscous flow: Buckling of planar jets, Int. J. Numer. Methods Fluids **29**, 705 (1999).
[5] D. H. Reneker and A. L. Yarin, Bending instability of electrically charged liquid jets of polymer solutions in electrospinning, J. Appl. Phys. **87**, 4531 (2000).
[6] T. Han, D. H. Reneker, and A. L. Yarin, Buckling of jets in electrospinning, Polymer **48**, 6064 (2007).
[7] N. M. Ribe, J. R. Lister, and S. Chiu-Webster, Stability of a dragged viscous thread: Onset of "stitching" in a fluid-mechanical "sewing machine," Phys. Fluids **18**, 124105 (2006).
[8] S. Chiu-Webster and J. R. Lister, The fall of a viscous thread onto a moving surface: A "fluid-mechanical sewing machine," J. Fluid Mech. **569**, 89 (2006).
[9] G. I. Taylor, in *Proceedings of the 12th International Congress of Applied Mechanics.* (Springer, New York, 1968).
[10] M. Le Merrer, D. Quéré, and C. Clanet, Buckling of Viscous Filaments of a Fluid Under Compression Stresses, Phys. Rev. Lett. **109**, 064502 (2012).
[11] M. Maleki, M. Habibi, R. Golestanian, N. M. Ribe, and D. Bonn, Liquid Rope Coiling on a Solid Surface, Phys. Rev. Lett. **93**, 214502 (2004).
[12] M. Habibi, Y. Rahmani, D. Bonn, and N. M. Ribe, Buckling of Liquid Columns, Phys. Rev. Lett. **104**, 074301 (2010).
[13] J. O. Cruickshank, Low-Reynolds-number instabilities in stagnating jet flows, J. Fluid Mech. **193**, 111 (1988).
[14] J. Cruickshank and B. Munson, The viscous-gravity jet in stagnation flow, J. Fluids Eng. **104**, 360 (1982).
[15] M. Matovich and J. Pearson, Spinning a molten threadline: Steady-state isothermal viscous flows, Ind. Eng. Chem. Fundam. **8**, 512 (1969).
[16] S. M. Suleiman, Viscous buckling of thin fluid layers, Phys. Fluids **24**, 1 (1981).
[17] N. M. Ribe, Periodic folding of viscous sheets, Phys. Rev. E **68**, 036305 (2003).
[18] N. M. Ribe, Coiling of viscous jets, Proc. R. Soc. A **460**, 3223 (2004).
[19] L. Mahadevan and J. B. Keller, Coiling of flexible ropes, Proc. R. Soc. A **452**, 1679 (1996).
[20] L. Mahadevan, W. Ryu, and A. Samuel, Fluid "rope trick" investigated, Nature (London) **392**, 140 (1998).
[21] J. O. Cruickshank, An energy loss coefficient in fluid buckling, Phys. Fluids **25**, 1935 (1982).
[22] N. M. Ribe, H. E. Huppert, M. A. Hallworth, M. Habibi, and D. Bonn, Multiple coexisting states of liquid rope coiling, J. Fluid Mech. **555**, 275 (2006).
[23] M. Habibi, M. Maleki, R. Golestanian, N. M. Ribe, and D. Bonn, Dynamics of liquid rope coiling, Phys. Rev. E **74**, 066306 (2006).
[24] T. Cubaud and T. Mason, Folding of Viscous Threads in Diverging Microchannels, Phys. Rev. Lett. **96**, 114501 (2006).
[25] T. Cubaud, B. M. Jose, and S. Darvishi, Folded microthreads: Role of viscosity and interfacial tension, Phys. Fluids **23**, 042002 (2011).
[26] T. Cubaud and T. G. Mason, Interacting viscous instabilities in microfluidic systems, Soft Matter **8**, 10573 (2012).
[27] M. M. Hohman, M. Shin, G. Rutledge, and M. P. Brenner, Electrospinning and electrically forced jets. I. Stability theory, Phys. Fluids **13**, 2201 (2001).
[28] Y. Yang, Z. Jia, J. Liu, Q. Li, L. Hou, L. Wang, and Z. Guan, Effect of electric field distribution uniformity on electrospinning, J. Appl. Phys. **103**, 104307 (2008).
[29] Y. Song, Z. Liu, T. Kong, and H. Shum, Manipulation of viscous all-aqueous jets by electrical charging, Chem. Commun. (Cambridge) **49**, 1726 (2013).
[30] M. Hashimoto, P. Garstecki, H. A. Stone, and G. M. Whitesides, Interfacial instabilities in a microfluidic Hele-Shaw cell, Soft Matter **4**, 1403 (2008).
[31] See Supplemental Material at http://link.aps.org/supplemental/10.1103/PhysRevApplied.3.034010 for details about the definition of jet slenderness and the jet expansion ratio, a phase diagram of jet folding with an aqueous-aqueous liquid system, a video recording jet transition from folding to unfolding, and an investigation of the role of electrical conductivities.
[32] A. S. Utada, E. Lorenceau, D. R. Link, P. D. Kaplan, H. A. Stone, and D. A. Weitz, Monodisperse double emulsions

generated from a microcapillary device, Science **308**, 537 (2005).
[33] C. Chung, D. Choi, J. M. Kim, K. H. Ahn, and S. J. Lee, Numerical and experimental studies on the viscous folding in diverging microchannels, Microfluid. Nanofluid. **8**, 767 (2010).
[34] J. O. Cruickshank, Ph.D. thesis, Iowa State University, 1980.
[35] J. R. Melcher and G. I. Taylor, Electrohydrodynamics: A review of the role of interfacial shear stresses, Annu. Rev. Fluid Mech. **1**, 111 (1969).
[36] G. Riboux, Á. G. Marín, I. G. Loscertales, and A. Barrero, Whipping instability characterization of an electrified visco-capillary jet, J. Fluid Mech. **671**, 226 (2011).
[37] M. M. Hohman and G. Rutledge, Electrospinning and electrically forced jets. II. Applications, Phys. Fluids **13**, 2221 (2001).
[38] I. G. Loscertales, A. Barrero, M. Márquez, R. Spretz, R. Velarde-Ortiz, and G. Larsen, Electrically forced coaxial nanojets for one-step hollow nanofiber design, J. Am. Chem. Soc. **126**, 5376 (2004).
[39] A. Thiam, N. Bremond, and J. Bibette, Breaking of an Emulsion Under an ac Electric Field, Phys. Rev. Lett. **102**, 188304 (2009).
[40] I. Hayati, A. Bailey, and T. Tadros, Mechanism of stable jet formation in electrodynamic atomization, Nature (London) **319**, 41 (1986).